

## Instability and softening in a continuous bi-rod

Roberto Alessi, Laura Aliotta, Matteo Brunetti, Matteo Ciotti, Roberto Paroni, Marco Picchi Scardaoni

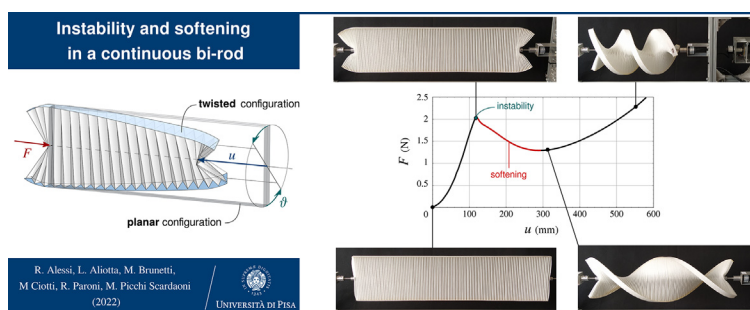
Department of Civil and Industrial Engineering, University of Pisa, Largo Lucio Lazzarino 1, 56122 Pisa, Italy



### HIGHLIGHTS

- The mechanical response of a continuous bi-rod structure composed of two flanges and a pleated web is investigated.
- The continuous bi-rod is characterised by an instability mechanism that couples axial contraction and twisting.
- The axial force–displacement response exhibits a significant softening phase.

### GRAPHICAL ABSTRACT



### ARTICLE INFO

#### Article history:

Received 19 July 2022

Revised 7 October 2022

Accepted 17 November 2022

Available online 23 November 2022

#### Keywords:

Bi-rod  
Instability  
Softening  
Pleated structures  
Compliant mechanisms

### ABSTRACT

We present a continuous bi-rod structure composed of two flanges and a pleated web. The structure is characterised by an instability mechanism that couples axial contraction and twisting. In so doing, the latter can be controlled by the former. Moreover, a remarkable softening response is observed immediately after the critical state. A custom testing machine has been designed and manufactured in order to experimentally investigate the mechanical response of the continuous bi-rod. Full scale finite element simulations have been also performed to provide a deeper understanding of the relative contribution of the flanges and the pleated web to the observed mechanical response. The features exhibited by the continuous bi-rod pave the way for innovative technological applications in areas of growing interest (e.g., compliant mechanisms, morphing and deployable structures).

© 2022 The Author(s). Published by Elsevier Ltd. This is an open access article under the CC BY-NC-ND license (<http://creativecommons.org/licenses/by-nc-nd/4.0/>).

## 1. Introduction

In recent years many efforts have been devoted to study the interplay between geometry and instability in structures and mechanisms, possibly at different scales, in order to exploit structures in all their complexity [1–4]. That is, the transition from “Buckliphobia” to “Buckliphilia” [5].

*Morphing structures*, i.e., structures that can adapt their configuration according to the operating conditions in order to improve their performance [6], strongly take advantage of this design con-

cept. As a matter of fact, morphing structures provide the possibility of realising functional shapes combining light-weight and load-bearing capabilities with simple mechanical design. This combination of features leads to a reduction of moving parts, a friction decrease, and allows to achieve multi-objective design, thus enhancing the overall efficiency. These characteristics have been attractive for several engineering fields, as, for instance, aerospace and robotics, where simplicity and versatility of the design offer many advantages, compared to traditional solutions [7–9].

A deeply investigated morphing structure is the double- or bi-rod, frequently met in nature and in human-made applications. This structural configuration may range from the nano- to the macro-scale [10,11]. In its simplest setup, it is composed of two

E-mail addresses: [roberto.alessi@unipi.it](mailto:roberto.alessi@unipi.it) (R. Alessi), [laura.aliotta@unipi.it](mailto:laura.aliotta@unipi.it) (L. Aliotta), [matteo.brunetti@unipi.it](mailto:matteo.brunetti@unipi.it) (M. Brunetti), [roberto.paroni@unipi.it](mailto:roberto.paroni@unipi.it) (R. Paroni), [marco.picchiscardaoni@ing.unipi.it](mailto:marco.picchiscardaoni@ing.unipi.it) (M. Picchi Scardaoni)

possibly prestressed flanges with rectangular cross-sections linked by rigid pinned spokes that keep constant the distance between the points they connect and leave unconstrained the relative rotation along the connecting direction.

This structural arrangement has been introduced in the literature and extensively studied by Weaver and co-workers [12–14] as a promising solution in the design of *deployable structures*, that is, structures capable of automatically varying their shape from a compact and packaged to an expanded and operational configuration [15] (see also [16] for a comprehensive overview of the possible applications, ranging from space structures to temporary architecture and medical devices).

Indeed, with a proper choice of geometry, prestress and anisotropy, the bi-rod can be designed to have multiple stable equilibrium configurations, of either straight or helical shape, including a completely folded one, while keeping the strains within the elastic limit. Therefore, by exploiting the multistability, the structure can meet its operational requirements by demanding power only to switch from one stable configuration to another, not to hold them, [18].

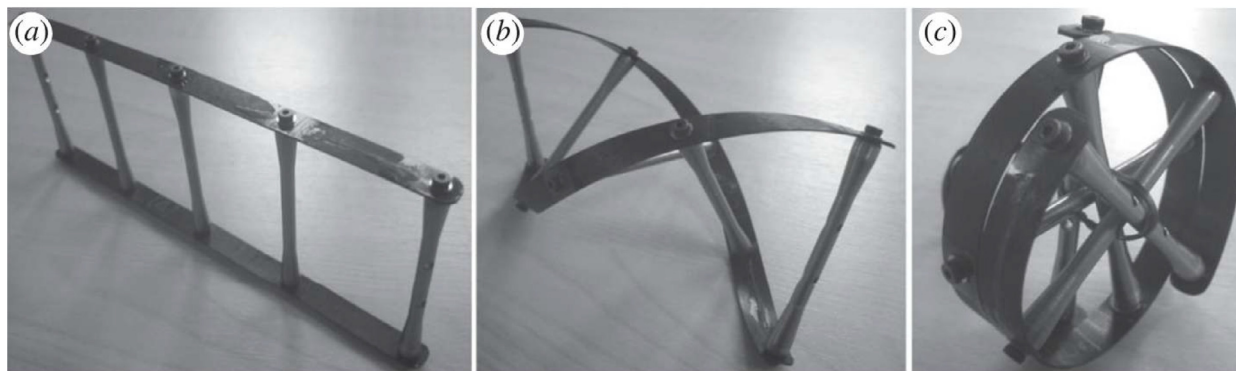
This bi-rod, hereafter referenced to as *discrete bi-rod* because of the finite number of spoke connections, is generally modeled as two elastic rods subjected to mutual kinematic constraints mimicking the effect of the pinned rigid spokes, Fig. 1i, [19–21]. That is, (in the aforementioned studies) the ‘web’ of the discrete bi-rod is treated as a rigid “filler” rather than as a component to be considered in the design. It is also the case of [11], where a version of the discrete bi-rod is studied for continuous linear actuation.

In this paper we propose a “continuous” version of the discrete bi-rod, hereafter referenced to as *continuous bi-rod*. Specifically, the

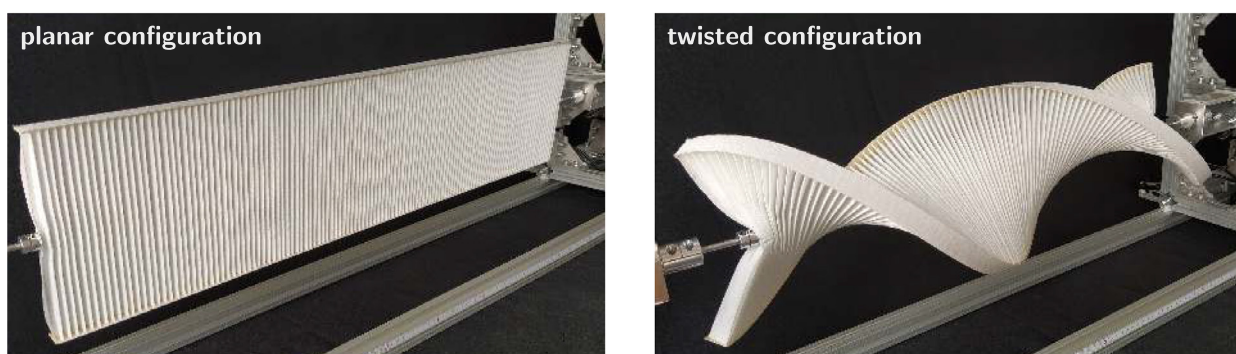
spokes are replaced by a flat foldable *pleated web* that provides a continuous constraint on the flanges, Fig. 1ii. *Pleated and foldable structures*, being able to fold and unfold along the creases, are frequently found in natural structural systems (insect wings, leaves, flower petals) and are well suited to design innovative deployable structures, as well as flexible mechanical metamaterials, [22–24].

A major difference between the discrete and the continuous bi-rod is that, while in the former the spokes are pinned to the rods and are free to rotate, in the latter the rotations of the flanges are coupled to those of the strips, thus providing a non-trivial coupling between geometry and elasticity. As it will be shown, this interplay has a major impact in the global mechanical response of the continuous bi-rod. Indeed, it provides a non-linear relationship between the axial displacement and the axial force capable of triggering an elastic instability that can be actively exploited to couple and control the overall axial contraction and twisting. It is worth remarking that a similar coupling mechanism has been also achieved in [25–27] by designing a specific three-dimensional metamaterial unit cell.

The continuous bi-rod inherits and improves the characteristics of its discrete counterpart: it can be folded into itself up to maximum compaction, depending either on the geometry of the flanges and the pleats. Even if it is out of the scope of the present paper, it could also be endowed with a tailored multi-stable behaviour using the same design solutions that have proven effective with the discrete bi-rod, that is, prestressing the flanges and/or tailoring their anisotropy. Moreover, the continuous bi-rod presents many additional features if compared to its discrete counterpart, as the absence of discrete mechanisms/joints and the contraction-twisting coupling with a softening phase.



(i) The original discrete bi-rod, as developed in Weaver’s laboratory, in (a) straight, (b) twisted and (c) coiled configuration (figure taken from [13] and reproduced with authorization).



(ii) The continuous bi-rod provided by AIR TOP ITALIA Srl company [17] in its planar (left) and twisted (right) configuration.

**Fig. 1.** Overall views of the discrete and continuous bi-rods. The latter conceptually obtained from the former by replacing the discrete pinned spokes with a continuous pleated web.

Concerning the absence of discrete mechanisms/joints, the continuous bi-rod rightly belongs also to the class of *compliant mechanisms*, that is, flexible mechanisms that transmit force and motion through the deformation of elastic members, usually localised, in contrast with the usual rigid-body joints. It has been widely shown that compliant mechanisms can achieve complex motions from simple topologies [28,29]. The interest in this class of mechanisms has been very recently promoted by Kirigami, the Japanese art of cutting paper [2,30].

Concerning the mechanical response, an unconventional buckling phenomenon that couples axial contractions and helical twist, with an axial force–displacement behaviour exhibiting a remarkable post-critical softening phase, is observed. These features can be exploited for multiple applications, such as energy absorbers or damper devices, [31], paving the way for a new concept of soft compliance devices.

The rest of the paper is structured as follows. Section 2 presents the investigated continuous bi-rod. Section 3 details the experimental setup while Section 4 illustrates the modeling aspects undertaken by finite element analyses. The results of the experimental testing and the finite element analyses are compared in Section 5, where the coupling between contraction and twisting is assessed. Concluding remarks are finally drawn in Section 6, where potential applications are also mentioned.

## 2. The continuous bi-rod: geometry and material properties

The continuous bi-rod prototype considered in this work has been provided by the Research and Development department of AIR TOP ITALIA Srl, [17], a leader Italian company in the production of automotive cabin air pollution filters.

The pleated web is made up of a relatively soft non-woven polymeric fabric regularly folded with constant pitch, whereas the two flanges consist of a significantly stiffer non-woven polymeric fabric ribbon of rectangular cross-section. The pleated web core and the two flanges are glued together with an industrial hot-melt adhesive. The geometry of the continuous bi-rod and its components are highlighted in Fig. 2; dimensions are reported in Table 1 together with the associated material elastic properties. The material of both the flanges and the pleated web has been considered as a linear elastic isotropic material. The Young's modulus of the flange and of the pleated web have been experimentally deter-

mined from small specimens cut out from the continuous bi-rod and tested with respect to directions highlighted in Fig. 2.

## 3. Experimental setup

A graphical representation of the test setup is depicted in Fig. 3, where the notation is also introduced. Accordingly, the midpoint of the first leftmost strip of the pleated web, point  $P$ , is kept fixed. At the same point, the rotation around the three axes is impeded, as well. Conversely, a monotonically increasing displacement is prescribed at the rightmost strip midpoint  $Q$ , directed along  $-\mathbf{e}_3$ . Moreover, the midpoint  $Q$  is left free to rotate around  $\mathbf{e}_3$  whereas the rotations around the other two axes are constrained. Controlling the applied axial displacement at  $Q$ , the mechanical response of the continuous bi-rod is described by the reactive force  $F$  at  $P$ , directed along  $\mathbf{e}_3$ , and by the twist rotation  $\vartheta$  at  $Q$ .

An in-house custom testing machine has been designed and manufactured in order to implement the aforementioned test setup. As highlighted in Fig. 4, the testing machine consists of a fixed outer frame and a moving inner frame. Both are made of standard T-Slot aluminium profiles, with the inner frame sliding on glides in the grooves of the longitudinal elements of the outer frame. A longitudinal displacement actuation is obtained with a double axis electric motor mounted on the inner frame and linked through an endless screw with a thrust bearing to the outer frame. On the second axis, a rotary encoder allows to record and control motor rotations and, consequently, the moving frame advancement, with a resolution of  $\pm 0.03\text{mm}$ . On the inner frame, opposite to the endless screw, a second rotary encoder allows for the recording of the rotation  $\vartheta$ , corresponding to the overall bi-rod twist rotation, with a resolution of  $\pm 0.075^\circ$ . On the fixed outer frame end, a 10N load cell is mounted, allowing for the determination of the reaction force  $F$ . All the electronics and acquisition unit, based on Arduino UNO Rev3 [32], have been designed and realised in-house, allowing for real-time data reading.

## 4. The finite element model

Numerical finite element investigations have been performed with Abaqus FEA software [33], in order to reproduce the experimental results and highlight the key factors affecting the global response. Specifically, a parametric Python script has been developed for the set up of the model.

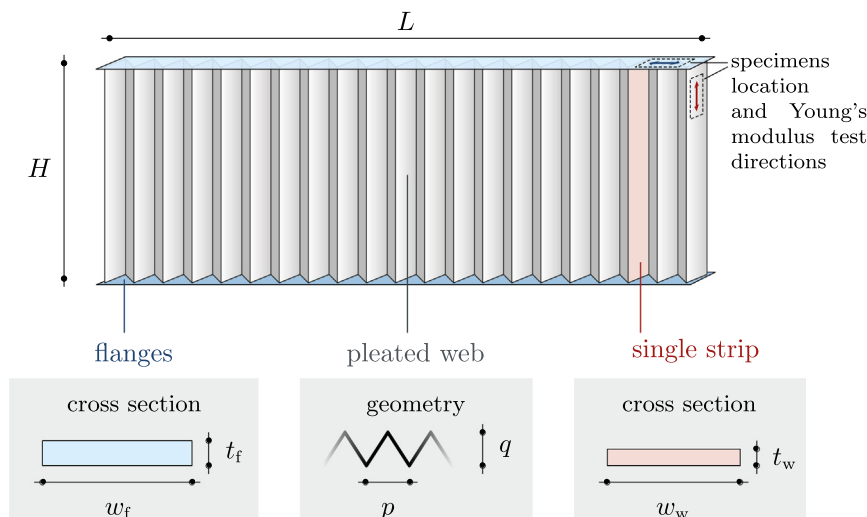
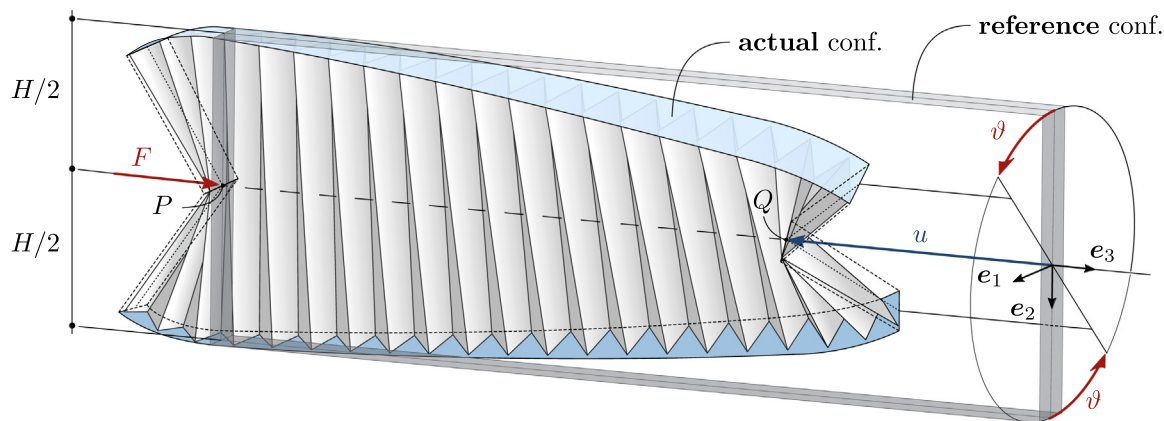


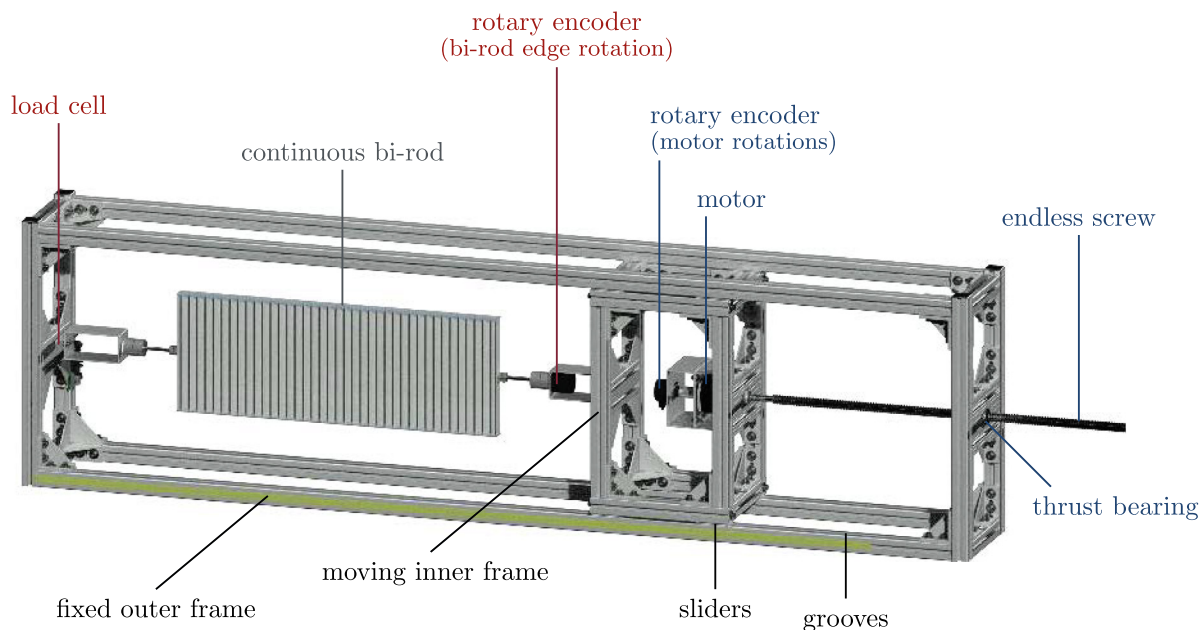
Fig. 2. Geometry and dimensions of the continuous bi-rod and its components.

**Table 1**  
Geometry and material properties of the continuous bi-rod and its components.

continuous bi-rod	geometry	$L$	902	mm
		$H$	209	mm
flanges	geometry	$w_f$	22	mm
		$t_f$	1.75	mm
	material	$E_f$	179.9	MPa
		$\nu_f$	0.25	-
		$G_f$	72.0	MPa
pleated web	geometry	$w_w$	19.8	mm
		$t_w$	0.58	mm
		$p$	7.4	mm
		$q$	19.5	mm
		material	$E_w$	161.3
	$\nu_w$		0.25	-
			$G_w$	64.5



**Fig. 3.** Test setup with controlled axial displacement (blue) and monitored axial force and twist rotation (red).



**Fig. 4.** Overall view and details of the testing machine: (black) frame parts, (blue) parts involved in the actuation, (red) sensors involved in the test outcome data.

Geometric and material properties used in the simulations are those reported in Table 1. The finite element model of the continuous bi-rod is depicted in Fig. 5, where details of the flanges and of

the pleated web modeling are highlighted. Each strip is meshed by 168 S4R elements (linear four-node six degree of freedom per node shell elements, with reduced integration): 4 elements in the short

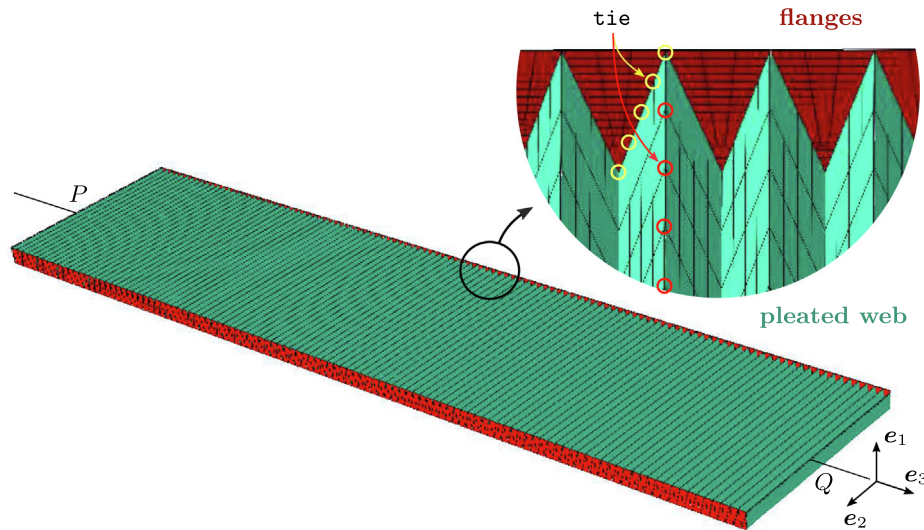


Fig. 5. Finite element model and mesh details.

direction and 42 in the long. Each flange is meshed by about 11 000 S4R and S3R (triangular counterpart of S4R) elements. The overall model is composed of about 300 000 elements. The final mesh size is a result of a convergence study, not reported here for the sake of brevity.

Since strips and flanges are independent instances in the assembly, some degrees of freedom have been constrained, so to model the flange-web gluing and the foldable creases between strips. Specifically, the strips are tied to the flanges via node-to-node tie, constraining all the six degrees of freedom of the correspondent nodes, as shown in Fig. 5 (yellow circles). Nodes along the long edges of the strips are similarly tied, but only for the translational degrees of freedom (red circles in Fig. 5), to create perfect hinges along the creases of the resulting pleated web. Indeed, an uniaxial compaction test, carried out only on the pleated web, has unveiled the fact that the creases stiffness is very small and the crease folding contribution to the global response negligible. This should be of no surprise since the material at the creases is highly plasticised and damaged. The mesh is generated to guarantee the node-to-node correspondence of the tied nodes.

A hard pressure-overclosure relationship without friction has been specified in the model, so to avoid unphysical interpenetration of components.

The boundary conditions are conceptually the same as described in Section 3. The node corresponding to point P is clamped, whilst the node corresponding to point Q can only move along the  $e_3$  direction (see Fig. 3) and rotate along the same axis. At this node, the prescribed displacement is applied.

The analysis is solved by the Abaqus/Standard dynamic implicit solver, with quasi-static and nlgeom (geometric

non-linearity) options activated. The final imposed displacement is 600mm, reached with a constant rate. The maximum integration time step has been set to 1.5s.

A small geometrical imperfection through a perturbation of the mesh nodal coordinates has been considered, in order to allow the numerical model to follow the non-trivial equilibrium path. This perturbation has been obtained by superimposing the first mode of vibrating of the free-body model, normalised by its maximum value (see Fig. 6) and multiplied by a factor 0.1mm, to the nodal coordinates of the flat reference configuration, before the beginning of the analysis. The modal analysis is carried out upstream, and the results are directly passed to the quasi-static solver via \*imperfection option.

## 5. Results

In this Section, we compare and comment experimental and numerical results at once.

According to the experimental setup described in Section 3, we have performed five experimental tests with an applied displacement rate of 0.9mm/min, corresponding to  $0.001s^{-1}$  of axial contractive strain rate.

We solved the numerical model described in Section 4 on a workstation with Intel® Core™ i9-9940X CPU @ 3.30GHz and 64GB RAM with two processors dedicated to the solver. Since reduced integration elements have been used, we made sure that the artificial energy (ALLAE), introduced in the element formulation to avoid spurious deformation modes, is small if compared to the elastic strain energy. It results that the former is less than 0.1% of the latter.

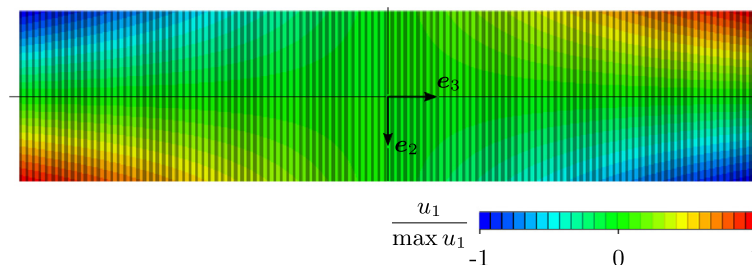
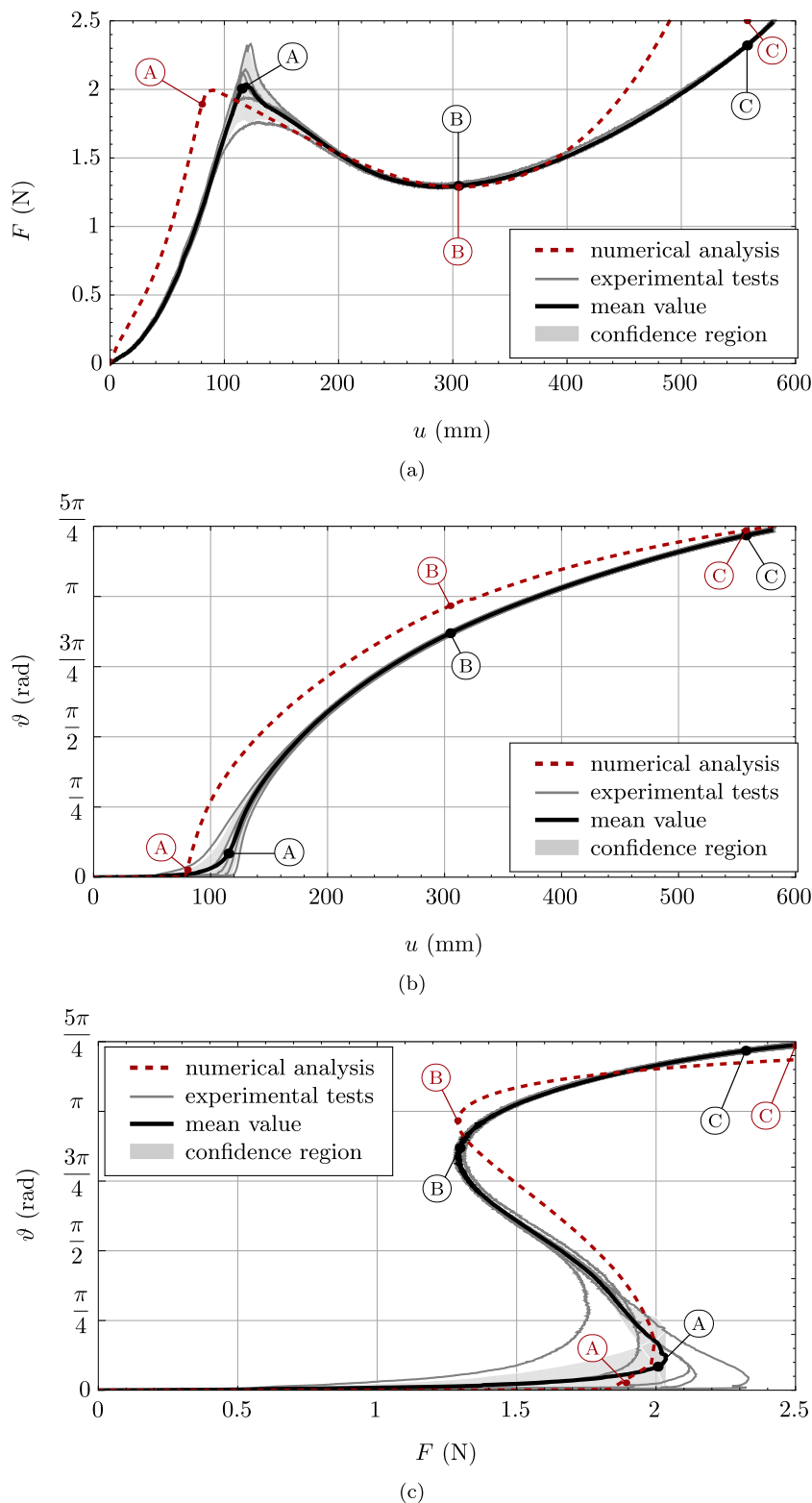


Fig. 6. First mode of vibrating (out-of-plane displacement colormap) used as mesh perturbation for initial geometry imperfection.




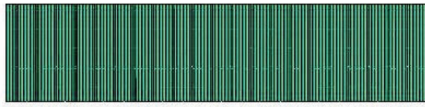

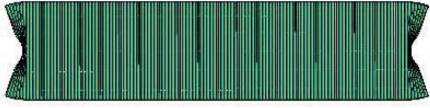

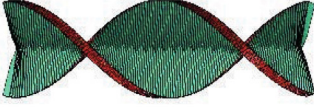


**Fig. 7.** Experimental and numerical results: (7a) force–displacement, (7b) twist–displacement and (7c) twist–force responses. The noteworthy states A, B and C correspond to the configurations highlighted in figures of Table 2.

The force–displacement ( $F-u$ ), twist–displacement ( $\vartheta-u$ ) and twist–force ( $\vartheta-F$ ) responses obtained from the experiments and finite element analysis are compared in Fig. 7, where we reported the five-test results together with their mean value and confidence region (95%), and the finite element solution. Key states of the

response are denoted by labels O, A, B, C, with the associated configurations reported in Table 2.

With reference to these outcomes, we note that the structure remains in an approximately planar configuration up to state A. From that state on, rotations start to evolve significantly, and

**Table 2**  
Comparison of experimental and numerical configurations corresponding to the significant states highlighted in Fig. 7.

(O) (ref. conf.)		
(A)		
(B)		
(C)		

the structure assumes a twisted configuration. Up to state A, the force–displacement behaviour is almost linear, apart from an initial transient stage, less evident in the numerical simulation, which is probably due to the initial compaction of the first strips. We recall that the specimens are not originally meant to be mechanically tested. A uniform progressive compaction is observed only after a few of the outermost couples of strips, typically four or five, got in touch. At state A and immediately after, the structure rapidly begins to twist into itself, denoting that the planar configuration becomes unstable and, consequently, the occurrence of a bifurcation of the trivial, planar equilibrium path. Quite surprisingly, after state A, whilst the imposed displacement increases, the force needed to maintain equilibrium decreases up to a local minimum denoted by label B. We explain this softening behaviour by local relaxation of the outermost regions of the bi-rod pleated web, due to the exploration of non-planar and energetically-favourable configurations. The quantity

$$\Lambda := \frac{F_B - F_A}{F_A},$$

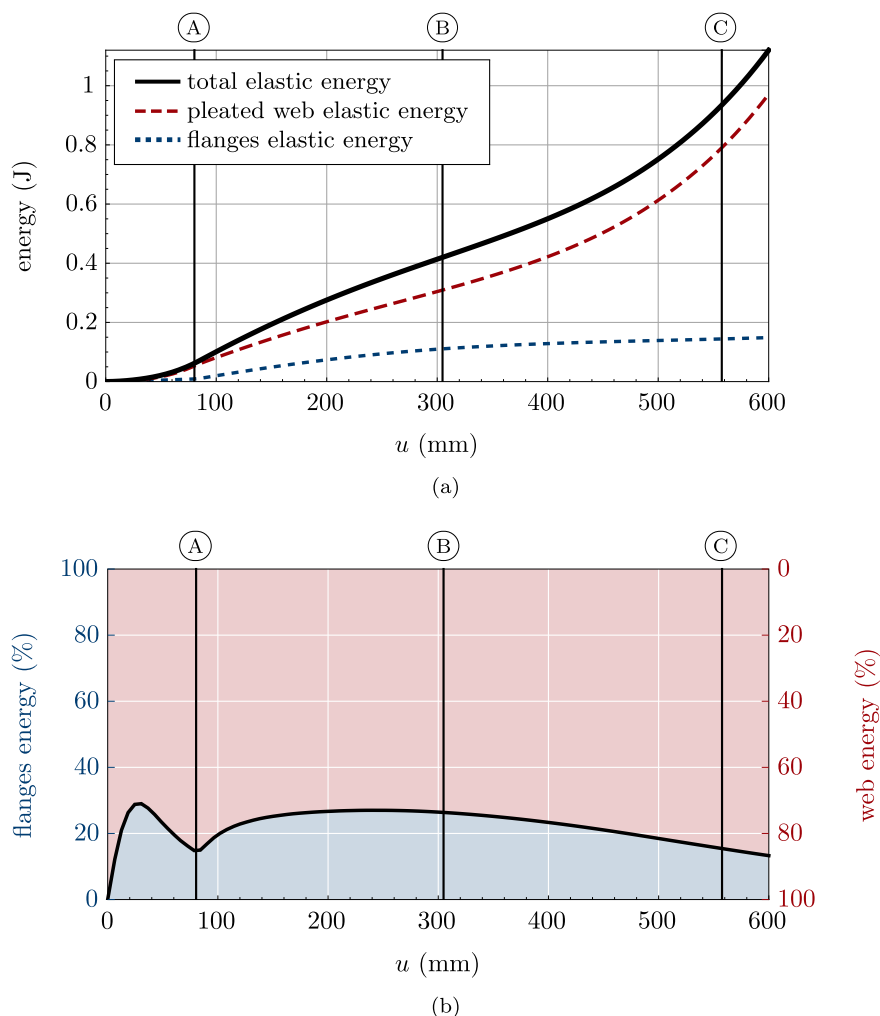
representing the relative variation of the reactive force between the new minimum value after relaxation and the force peak value, is related to the energy absorption capabilities of the structure. In the present case,  $\Lambda \approx -35\%$ ; this force decay can be exploited for energy absorption purposes, as later discussed in Section 6. At the same time, the bi-rod continues to twist into a double-helical. After state B, the reactive force has again a positive monotone trend with the increasing imposed displacement, and the bi-rod begins to compact. In this phase, the finite element solution overestimates the reactive force. We reckon that this fact is due to a not extremely accurate modeling of the contact behaviour among strips in the highly-compacted regime, and to a non-linear behaviour of the material in the highly deformed regions. Moreover, the gluing

between strips and flanges can also contribute to lowering the stress. From state A on, contractions are converted into twist. State C corresponds to compaction of the bi-rod up to almost 65% of its initial length.

From Table 2, where the deformed shapes of the actual continuous bi-rod and of the finite element results are put side-by-side for each highlighted state, it can be appreciated the good agreement between experiments and numerics. Remarkably, the finite element model is able to predict all the salient features of the observed structure response.

The finite element simulations, differently from the experiments, allow us to quantify the contribution of the flanges and the pleated web with respect to the overall response. The elastic energy stored in the flanges and in the pleated web as a function of the imposed displacement is shown in Fig. 8a, while the relative contribution in percentage terms is highlighted in Fig. 8b. Both contributions are monotonically increasing and the flanges energy asymptotically tends to a constant value. In addition, its mean relative contribution is about 20% of the total, whilst its maximum is no more than 30%.

The energetic contributions and their relative variations provide useful insights for the understanding of the mechanical response. In the first phase (O–A) the load, directly applied to the outermost strips, is gradually transferred to the flanges, whose relative energy contribution increases up to its maximum value. This trend reverses when the strips begin to pack while undergoing a localised bending: immediately before the occurrence of the instability. The energy percentage contribution of the pleated web increases up to approximately 85%. In the second phase (A–B), following the twisting instability, the relative energy contribution of the flanges slightly increases again. This is due to a partial relaxation of the localised bending of the outermost strips, whose manifestation in the global response is the onset of softening. Finally, in the third phase (B–C), the relative energy contribution of the pleated



**Fig. 8.** Absolute (8a) and relative (8b) numerical contributions to the total elastic energy of the flanges (blue) and the pleated web (red). The circled labels identify the states in Table 2.

web returns to increase. This is attributable to the compaction of the internal strips, which induces a recovery of axial stiffness, and corresponds to the second hardening stage.

## 6. Conclusions

In this work we presented a continuous bi-rod that exploits instability to convert axial contraction into twisting. It is composed by two flanges and a continuous pleated web. We characterised the response of the structure both experimentally, with an in-house manufactured testing machine, and numerically, via finite element simulations. We showed that the response to axial contraction is non-trivial. Specifically, after an initial monotone relationship between contraction and reactive force, a bifurcation of the fundamental equilibrium path occurs. The non-trivial equilibrium path is characterised by helical-twisted configurations and by a softening-hardening force-displacement response.

The continuous bi-rod belongs to many classes of structures and mechanisms. It is a morphing structure, because it can achieve different configurations through a global deformation process. It can be labelled also as foldable structure, thanks to the creases of the pleated web. In addition, the absence of traditional rigid and punctual joints makes the continuous bi-rod a compliant mechanism.

As far as the possible applications of this structure are concerned, multiple possibilities arise, owing to the versatility of the

continuous bi-rod. The conversion of axial contraction and twist, joined to the absence of traditional mechanisms, can be exploited for actuations purposes, especially in soft robotics and micro-/nano-robotics. This structure could also be used for developing a metamaterial for energy dissipation and damping. Motivated by the widely-spread presence of helical patterns in nature, at different scales, it could be significant, in this sense, to study the properties of a lattice structure where the representative cell is represented by a properly designed continuous bi-rod. Moreover, the possibility to include a multi-stable behaviour, for example with a simple pretension of the structure centre line or by exploiting anisotropy and flanges prestress, opens opportunities in the context of multi-stability, such as energy absorption and release [31]. It is the case, for instance, of the chameleon tongue: its quick and efficient unravel, releasing previously-stored energy, is ruled by structural helical patterns [34,35].

Future work will also address the analytical mechanical modeling of the continuous bi-rod, so to provide a self-contained predictive model as the geometrical and material parameters may change. Research is ongoing in this sense.

## Data availability

Data will be made available on request.



## Declaration of Competing Interest

The authors declare that they have no known competing financial interests or personal relationships that could have appeared to influence the work reported in this paper.

## Acknowledgements

The Authors warmly thank AIR TOP ITALIA Srl company, in particular Eng. Lorenzo MAZZOCANTI from the Research and Development division, for its support in providing the tested specimens, and the Multifunctional Bio-Ecocompatible Materials Laboratory of the University of Pisa, directed by Prof. Andrea LAZZERI, where the raw materials for their mechanical characterisation have been tested.

RA, MB, RP, and MPS acknowledge the support of the Italian National Group of Mathematical Physics INdAM-GNFM. RA, MB, RP, and MPS also acknowledge the support of the Project PRIN 2017 20177TTP3S.

RA, LA, MB, and RP acknowledge the support from the University of Pisa through the project PRA\_2022\_69 "Advanced modelling of ultra-lightweight materials and structures".

RA is also sincerely grateful to Prof. Giuseppe RUTA for the first insightful discussions on the topic.

## References

- [1] J. Shim, C. Perdigou, E.R. Chen, K. Bertoldi, P.M. Reis, Buckling-induced encapsulation of structured elastic shells under pressure, *Proc. Natl. Acad. Sci.* 109 (16) (2012) 5978–5983, ISSN 0027–8424, doi: 10.1073/pnas.1115674109, <https://pnas.org/doi/full/10.1073/pnas.1115674109>.
- [2] A. Rafsanjani, Y. Zhang, B. Liu, S.M. Rubinstein, K. Bertoldi, Kirigami skins make a simple soft actuator crawl, *Sci. Robot.* 3 (15), ISSN 2470–9476, doi: 10.1126/scirobotics.aar7555, <https://www.science.org/doi/10.1126/scirobotics.aar7555>.
- [3] J. Marthelot, P.-T. Brun, F.L. Jiménez, P.M. Reis, Reversible patterning of spherical shells through constrained buckling, *Phys. Rev. Mater.* 1 (2) (2017) 025601, ISSN 2475–9953, doi: 10.1103/PhysRevMaterials.1.025601, URL <http://link.aps.org/doi/10.1103/PhysRevMaterials.1.025601>.
- [4] S. Chibbaro, W. Hamouche, C. Maurini, S. Vidoli, A. Vincenti, Chaotic and regular dynamics of a morphing shell with a vanishing-stiffness mode, *Extreme Mech. Lett.* 54 (2022) 101755, <https://doi.org/10.1016/j.eml.2022.101755>, <https://linkinghub.elsevier.com/retrieve/pii/S2352431622000918>.
- [5] P.M. Reis, A Perspective on the Revival of Structural (In)Stability With Novel Opportunities for Function: From Buckliphobia to Buckliphilia, *J. Appl. Mech.* 82 (11), ISSN 0021–8936, doi: 10.1115/1.4031456, <https://asmedigitalcollection.asme.org/appliedmechanics/article/doi/10.1115/1.4031456/474193/A-Perspective-on-the-Revival-of-Structural>.
- [6] Y. Li, S. Pellegrino, A Theory for the Design of Multi-Stable Morphing Structures, *J. Mech. Phys. Solids* 136 (2020) 103772, ISSN 00225096, doi: 10.1016/j.jmps.2019.103772, URL <https://linkinghub.elsevier.com/retrieve/pii/S0022509619307628>.
- [7] S. Carey, C. Mchale, V. Oliveri, P.M. Weaver, Reconfigurable helical lattices via topological morphing, *Mater. Des.* 206, doi: 10.1016/j.matdes.2021.109769.
- [8] C. McHale, D.A. Hadjiloi, R. Telford, P.M. Weaver, Morphing composite cylindrical lattices: Enhanced modelling and experiments, *Journal of the Mechanics and Physics of Solids* 135 (2020) 103779, ISSN 00225096, doi: 10.1016/j.jmps.2019.103779, URL <https://linkinghub.elsevier.com/retrieve/pii/S0022509619301656>.
- [9] A. Pirrera, X. Lachenal, S. Daynes, P.M. Weaver, I.V. Chenchiah, Multi-stable cylindrical lattices, *J. Mech. Phys. Solids* 61 (11) (2013) 2087–2107, <https://doi.org/10.1016/j.jmps.2013.07.008>, <https://linkinghub.elsevier.com/retrieve/pii/S0022509613001385>, ISSN 00225096.
- [10] Y.M. Tseytlin, Advanced Mechanical Models of DNA Elasticity, 2016.
- [11] A.P. Sabelhaus, K. Zampaglione, E. Tang, L.-H. Chen, A. Agogino, A. Agogino, Double-Helix Linear Actuators, *J. Mech. Des.* (2021) 1–40, <https://doi.org/10.1115/1.4050739>, ISSN 1050–0472.
- [12] A.F. Arrieta, V. van Gemmeren, A.J. Anderson, P.M. Weaver, Dynamics and Control of Twisting Bi-Stable Structures, *Smart Mater. Struct.* 27 (2) (2018) 025006.
- [13] X. Lachenal, P.M. Weaver, S. Daynes, Multi-stable composite twisting structure for morphing applications, *Proceedings of the Royal Society A: Mathematical, Physical and Engineering Science* 468 (2012) 1230–1251, doi: 10.1098/rspa.2011.0631, doi: 10.1098/rspa.2011.0631.
- [14] X. Lachenal, P.M. Weaver, S. Daynes, Influence of transverse curvature on the stability of pre-stressed helical structures, *International Journal of Solids and Structures* 51 (13) (2014) 2479–2490, ISSN 00207683, doi: 10.1016/j.ijsolstr.2014.03.014, doi: 10.1016/j.ijsolstr.2014.03.014.
- [15] S. Pellegrino (Ed.), *Deployable Structures*, Springer Vienna, Vienna, 2001, <https://doi.org/10.1007/978-3-7091-2584-7>, ISBN 978-3-211-83685-9.
- [16] G.E. Fenci, N.G. Currie, Deployable structures classification: A review, *Int. J. Space Struct.* 32 (2) (2017) 112–130, <https://doi.org/10.1177/0266351117711290>, <http://journals.sagepub.com/doi/10.1177/0266351117711290>, ISSN 0956–0599.
- [17] Air Top Italia Srl, <https://www.airtopitalia.com>, 2022.
- [18] M. Brunetti, A. Favata, S. Vidoli, Enhanced models for the nonlinear bending of planar rods: localization phenomena and multistability, *Proceedings of the Royal Society A: Mathematical, Physical and Engineering Sciences* 476 (2242) (2020) 20200455, ISSN 1364–5021, doi: 10.1098/rspa.2020.0455, <https://royalsocietypublishing.org/doi/10.1098/rspa.2020.0455>.
- [19] T. Lessinnes, A. Goriely, Design and stability of a family of deployable structures, *SIAM Journal on Applied Mathematics* 76 (5) (2016) 1920–1941, <https://doi.org/10.1137/16M1070293>, ISSN 00361399.
- [20] D.E. Moulton, T. Lessinnes, A. Goriely, Morphoelastic rods. Part I: A single growing elastic rod, *Journal of the Mechanics and Physics of Solids* 61 (2) (2013) 398–427, ISSN 00225096, doi: 10.1016/j.jmps.2012.09.017, doi: 10.1016/j.jmps.2012.09.017, <https://linkinghub.elsevier.com/retrieve/pii/S0022509612002104>.
- [21] T. Lessinnes, D.E. Moulton, A. Goriely, Morphoelastic rods Part II: Growing birods, *Journal of the Mechanics and Physics of Solids* 100 (September 2014) (2017) 147–196, ISSN 00225096, doi: 10.1016/j.jmps.2015.07.008, doi: 10.1016/j.jmps.2015.07.008, <https://linkinghub.elsevier.com/retrieve/pii/S0022509615300181>.
- [22] Z.Y. Wei, Z.V. Guo, L. Dudte, H.Y. Liang, L. Mahadevan, Geometric Mechanics of Periodic Pleated Origami, *Physical Review Letters* 110 (21) (2013) 215501, ISSN 0031–9007, doi: 10.1103/PhysRevLett.110.215501, URL <https://link.aps.org/doi/10.1103/PhysRevLett.110.215501>.
- [23] A. Lebé, From Folds to Structures, a Review, *Int. J. Space Struct.* 30 (2) (2015) 55–74, <https://doi.org/10.1260/0266-3511.30.2.55>, ISSN 0956–0599, <http://journals.sagepub.com/doi/10.1260/0266-3511.30.2.55>.
- [24] K. Bertoldi, V. Vitelli, J. Christensen, M. Van Hecke, Flexible mechanical metamaterials, *Nature Reviews Materials* 2 (11) (2017), <https://doi.org/10.1038/natrevmats.2017.66>, <http://www.nature.com/articles/natrevmats201766>, ISSN 20588437.
- [25] T. Frenzel, M. Kadic, M. Wegener, Three-dimensional mechanical metamaterials with a twist, *Science* 358 (6366) (2017) 1072–1074, <https://doi.org/10.1126/science.aao4640>, <https://www.sciencemag.org/lookup/doi/10.1126/science.aao4640>, ISSN 0036–8075.
- [26] C. Yang, K. Yang, Y. Tian, M. Fu, L. Hu, Theoretical analysis on the stiffness of compression–torsion coupling metamaterials, *Extreme Mechanics Letters* 46 (2021) 101336, <https://doi.org/10.1016/j.eml.2021.101336>, ISSN 23524316, <https://linkinghub.elsevier.com/retrieve/pii/S2352431621000997>.
- [27] H. Wang, C. Zhang, Q.-H. Qin, Y. Bai, Tunable compression–torsion coupling effect in novel cylindrical tubular metamaterial architected with boomerang-shaped tetrahedral elements, *Materials Today Communications* 31 (2022) 103483, <https://doi.org/10.1016/j.mtcomm.2022.103483>, <https://linkinghub.elsevier.com/retrieve/pii/S2352492822003518>.
- [28] L.L. Howell, *Compliant Mechanisms*, in: 21st Century Kinematics, Springer, London, London, 189–216, 2013, doi: 10.1007/978-1-4471-4510-3\_7, [http://link.springer.com/10.1007/978-1-4471-4510-3\\_7](http://link.springer.com/10.1007/978-1-4471-4510-3_7).
- [29] L.L. Howell, A. Midha, A Method for the Design of Compliant Mechanisms With Small-Length Flexural Pivots, *Journal of Mechanical Design* 116 (1) (1994) 280–290, ISSN 1050–0472, doi: 10.1115/1.2919359, <https://asmedigitalcollection.asme.org/mechanicaldesign/article/116/1/280/410458/A-Method-for-the-Design-of-Compliant-Mechanisms>.
- [30] A. Rafsanjani, K. Bertoldi, Buckling-induced kirigami, *Physical review letters* 118 (8) (2017) 084301.
- [31] Y. Cao, M. Derakhshani, Y. Fang, G. Huang, C. Cao, Bistable Structures for Advanced Functional Systems, *Adv. Funct. Mater.* 31 (45) (2021) 1–23, <https://doi.org/10.1002/adfm.202106231>, ISSN 16163028.
- [32] Arduino, <https://www.arduino.cc/>, 2022.
- [33] M. Smith, ABAQUS/Standard User's Manual, Version 6.9, Dassault Systèmes Simulia Corp, United States, 2009.
- [34] D.E. Moulton, T. Lessinnes, S. O'Keeffe, L. Dorfmann, A. Goriely, The elastic secrets of the chameleon tongue, *Proc. Roy. Soc. A: Math., Phys. Eng. Sci.* 472 (2188) (2016) 20160030.
- [35] J.H. de Groot, J.L. van Leeuwen, Evidence for an elastic projection mechanism in the chameleon tongue, *Proc. R. Soc. Lond. B Biol. Sci.* 271 (1540) (2004) 761–770.